STUDY OF $K_2SiF_6:Mn^{4+}@SiO_2$ PHOSPHOR FOR WHITE LEDS WITH HIGH ANGULAR COLOR UNIFORMITY

Sang Dang HO [1], *Nguyen Thi Phuong LOAN* [2], *Hsiao-Yi LEE* [3], *Nguyen Doan Quoc ANH* [1,*]

[1]Faculty of Electrical and Electronics Engineering, Ton Duc Thang University, Ho Chi Minh City, Vietnam.
[2]Faculty of Fundamental 2, Posts and Telecommunications Institute of Technology, Ho Chi Minh City, Vietnam.
[3] Department of Electrical Engineering, National Kaohsiung University of Science and Technology, Kaohsiung, Taiwan.

*Corresponding Author: Nguyen Doan Quoc ANH (Email: nguyendoanquocanh@tdtu.edu.vn)
(Received: 13-January-2024; accepted: 25-February-2024; published: 31-March-2024)
http://dx.doi.org/10.55579/jaec.202481.451

Abstract. *The distinctive wide-band blue illumination absorption and red strait-line discharge of the phosphor $K_2SiF_6:Mn^{4+}@SiO_2$ (KMnSF) make it an attractive material for manufacturing warm white light-emitting diodes (WLED). Nevertheless, using the highly corrosive raw ingredient HF to produce commercial KMnSF red phosphor has negative effects on the environment and people. In this study, microfluidic technology was used to successfully manufacture the KMnSF without the need for HF compound while resulting in a phosphor product with homogenous granule shape and size. The luminescence capabilities of the KMnSF samples were then thoroughly examined and characterized. Eventually, we made WLED packages comprising of blue LED chips, yellow phosphor $Y_3Al_5O_{12}:Ce^{3+}$ (YGA:Ce), red phosphor KMnSF, and SiO_2 scattering particle. Via varying the SiO_2 concentration during the simulation process, the prepared WLED's optical performances are obtained. The scattering properties of the phosphor layer as well as the lighting transmission and distribution were simulated with the utilization of both LightTools software and Monte Carlo theory. According to the outcomes, the microfluidic-synthesized $K_2SiF_6:Mn^{4+}$ proves to be appropriate for WLED apparatuses. Besides, the proposed phosphor compound with SiO_2 scattering particles showed the improvement in luminous flux and angular uniformity of the WLED.*

Keywords: WLED; $K_2SiF_6:Mn^{4+}$; Microfluidic technology; HF-free; Luminescence properties

1. Introduction

Great illuminating brightness, low power consumption, extended lifespan, and environmental protection have been key features for solid-state WLED devices to be recognized as a potential alternative for illumination uses [1, 2]. The device produces white ray by fusing one blue InGaN LED chip with one yellow phosphor called $Y_3Al_5O_12:Ce^3+$ (YGA:Ce) [3]. Nevertheless, its use in lighting and display is severely constrained by its poor hue rendering index (CRI) and elevated correlated color temperature (CCT) [4]. In order to change the corresponding hue temperature and then bring it to be

more consistent with natural illumination, the currently used way involves introducing phosphors that yield red elements.

Among various investigated red phosphors for WLEDs, scholars have recently become interested in the Mn4+ ion (not rare-earth) as it is possible to efficiently stimulate the ion via blue illumination (about 450 nm), emitting one strait-line red ray exhibiting one apex at around 630 nm, and subsequently enhance the illuminating performance for LED apparatuses significantly [5]. Numerous fluoride red phosphors incorporated with Mn^{4+} were described thus far, including K_2SiF_6:Mn^{4+} (KMnSF) phosphors that represent A_2XF_6:Mn^{4+} with A being Li, Na, K, Rb, Cs, NH4; and X being Si, Ge, Sn, Ti, Zr, Hf. The series of A_2XF_6:Mn^{4+} samples exhibit one smaller emitting line than the nitride red phosphor, accompanied by the emitting wavelength falling around 650 nm, matching the reception scope for our sight very well. According to numerous researches, these samples offer greater quantum yield. According to Chen *et al.* [6], K_2TiF_6:Mn^{4+} has inner quantum effectiveness of up to 98%, substantially surpassing nitride red phosphors.

Nevertheless, the majority of Mn^{4+} doped fluoride phosphors are necessarily prepared using hydrofluoric acid (HF), which is detrimental to human health [7, 8]. It is crucial to create one unique green combination method to aid in producing fluoride phosphors in red incorporated with Mn^{4+} in order to minimize or eliminate the use of HF. There have been several approaches to produce Mn^{4+}-doped fluorides using non-toxic liquids as alternatives to HF, such as NH_4F/HCl [14], NH_4F + HNO_3/HAc/H_3PO_4 [9], and H_3PO_4/KHF_2 [10]. In addition, another "green" method for synthesizing the K_2SiF_6:Mn^{4+} phosphor is the new microfluidic technology. The micro-liquid technique would be one significant strategy to aid in large-scale manufacturing in terms of practical implementations. The technique may accomplish steady as well as quick response, fitting fabrication in grand scope, in comparison to the conventional chemical combination approach. Additionally, it can obtain exact control over product size and form [11, 12].

In addition to accomplishing warm WLED, angular light uniformity is also an imperative feature for favorable WLED devices. Using only red phosphor is not an optimal approach to get better light-dispersion uniformity. Studies showed that the scattering in the LED package is one of the critical factors influencing the uniformity of angular light dispersion [13–15]. Thus, the study employs SiO_2 particles at nano-size as scattering regulators in the phosphor layer of the WLED. SiO_2 is one of the most investigated materials for enhancing scattering of photon and light extraction efficacy, leading to the increased external quantum efficacy of either quantum-dot LED or blue-pumped LED [16–18].

In this study, we employ the combination of yellow phosphor YGA:Ce, red phosphor KMnSF, and SiO_2 to reach the goal of enhancing color quality, both rendition and angular uniformity, for the blue-excited WLED package. The KMnSF is prepared with the micro-liquid technique to minimize the toxicity to the lowest level. The analysis of WLED's lighting properties is carried out with the adjustment in SiO_2 concentration. The optical simulation of the as-prepared WLED is performed using LightTools software and Monte Carlo theory. The Monte Carlo theory plays a critical role in our simulation and investigation of photon scattering and absorbing procedures [19]. In photon transport modeling, Monte Carlo has been recognized as the flexible method owing to its capability of producing high accuracy and handling 3D structures [20, 21]. As a result, Monte Carlo simulation is widely employed in sensing, imaging study, and biological fields involving light-medium interaction [22–24]. The simulation results shown that the small increase in SiO_2 concentration induces the luminous flux and angular uniformity of light output but the decrease in rendition performance. Such findings can be imperative references for further investigation on the use of SiO_2 and KMnSF phosphor in WLED development.

2. Experimental

2.1. Combination method

K_2SiF_6:Mn^{4+} phosphors were produced using microfluidic technology at room temperature. H_2SiF_6, KF, $KMnO_4$, HF, and KHF_2 made up the basic ingredients. Following Bode's procedure [25], the forerunner K_2MnF_6 was prepared. The details of raw ingredients are included in Table 1. The standard experimental operation procedure was demonstrated as follows: In one plastic beaker holding H_2SiF_6 along with another having ionized H_2O (2 ml), correspondingly, we applied K_2MnF_6 and KF, and both were agitated for 5 min. The solutions were drawn out of the two containers separately using the plastic syringes, added to the micro-liquid formation. The settings for the administering pump were established prior to the formation operation. The measuring magnitude along with administration rate parameters on both syringes are identical. In order to avoid sample buildup and air entering the pipeline, the equipment was positioned vertically. The material was gathered, and ethanol was used to wash it six times.

Tab. 1: Raw materials of Mn^{4+}-doped K_2SiF_6

Raw materials	Purity	Amount (in use)
H_2SiF_6	30-32%	2 ml 36 g in K_2MnF_6 precursor preparation;
KF	99%	2 mmol to combine with 0.06 mmol K_2MnF_6
$KMnO_4$	99.5%	2 g
HF	40%	150 ml
KHF_2	99%	2-12 g

2.2. WLEDs preparation

In Fig. 1 below, the specifications of WLEDs are presented. The WLED package used for simulation and testing comprised the blue-pumped LED chips and the phosphor layers of yellow phosphor YGA:Ce phosphor, red phosphor $K_2Si{F_6}$:Mn^{4+}incorporating SiO_2 particles (KMnSF@SiO_2). In the KMnSF@SiO_2 compound, KMnSF concentration is unchanged while the SiO_2 concentration is a variable, aiming at facilitating the scattering factor.

The presence of SiO_2 as scattering centers in the phosphor layer induces the change of YGA:Ce amount to keep the package stable throughout the simulation and testing process. In Figure 2, it shows the YGA:Ce phosphor dose based on SiO2 weight percentages. When the SiO_2 amount is 15 wt.%, the YGA:Ce dosage hits the lowest point at 26%. On the contrary, the YGA:Ce dosage reaches the highest points at 28 - 28.5% when the percentages of SiO_2 are approximately 2 wt.%. The YGA:Ce dosage rises when the weight percentages of SiO_2 decline.

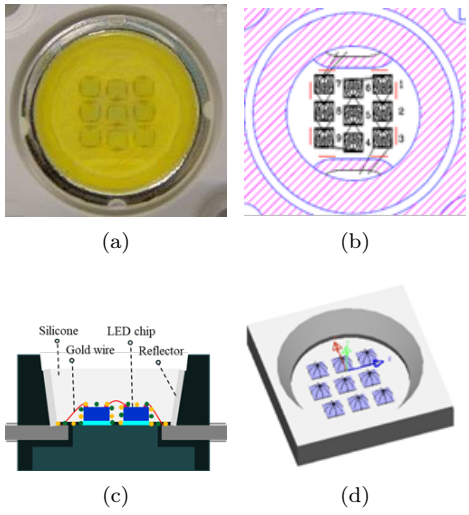

(a) (b) (c) (d)

Fig. 1: Images depicting WLED formation: (a) WLED apparatus, (b) Binding graph, (c) pc-WLEDs model visualized, (d) WLED device recreated via LightTools application.

2.3. Characterizations

The measurements for the as-prepared phosphor photoluminescence properties are listed in Table 2. One spectrophotometer was used to evaluate the diffuse reflectance spectrum in the UV-vis range. Using a fluorescence spectrometer, we captured the photoluminescence (PL) along with photoluminescent excitation (PLE) spectra. The identical set-up with an integration sphere was employed for the task of evaluating the quantum performance [26]. Spectrometer

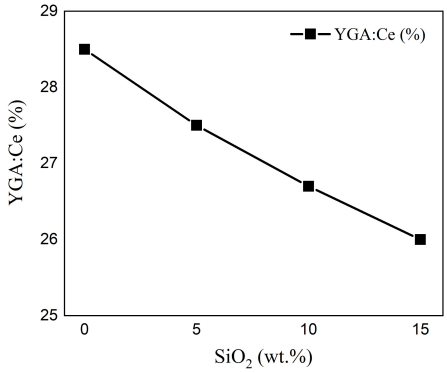

Fig. 2: The dosage of $YGA:Ce$ phosphor according to SiO_2 amounts.

data on the luminescence decay curve were collected. A LED photoelectric analyzer was used to record the electroluminescence characteristics of the WLEDs at one current reaching 30 milliamperes.

Tab. 2: Instruments for Mn^{4+}-doped K_2SiF_6 characteristic examination

Characteristics	Instruments	Models
UV diffuse reflection spectroscopy (DRS)	Spectro-photometer	UH4150 (Hitachi, Japan)
Photoluminescence & temperature-dependent emission spectra	Fluorescence Spectro photometer with a xenon lamp excitation source (150 W)	F-7000 (Hitachi, Japan)
Decay curve of luminescence	Spectro-fluorometer (via steady and transient states)	FS5 Spectrofluorometer (Edinburgh Instruments ,UK)

3. Results and Discussion

3.1. Simulation computation of the as-prepared red phosphor

The typical particle sizes are around 3.54, 3.65, 4.14, 3.85, and 3.67 m for injection rates of 500, 750, 1000, 1250, and 1500 μL/min, in turn. The administration rate of 1000 μL/min leads to the most homogeneous particle size dispersion. In a fluid reaction, the reacting criteria significantly alter the substances' form. The equation below serves as an illustration of this [27]:

$$Q = \frac{2Q_v}{\pi d^2/4} \tag{1}$$

where Q_v signifies the administration rate along with the volume flux from one administrating pipe. d signifies the duct's diameter. Q signifies the volume flux for each unit zone within the duct. Q would be clearly influenced by d and Q_v and is connected to the reaction circumstances. The aforementioned events demonstrate how microfluidic technology's settings may be changed to efficiently manage the size dispensation of specimens [28].

$$I_t = I_0 + Ae^{(-t/\tau)} \tag{2}$$

where I_t and I_0 represent, accordingly, the illumination strength at time t and 0. While τ is the fluorescence lifespan, A is a constant. In accordance with the pattern of spectral variation, the predicted lifespan of specimens with administration rates measured at 500, 750, 1000, 1250, and 1500 μL/min would be 8.62, 9.22, 9.29, 9.14, and 9.01 ms, in turn.

The luminescence quantum yields (PLQY) of K_2SiF_6:Mn^{4+} achieved at various injection speeds have been studied in order to better investigate the reasons for illumination strength changes. The radioactive along with non-radioactive repeated mixing speed for the specimens were determined by mixing the findings of PLQYs and luminous lifespan. The proportion of photons released to photons absorbed is known as the PLQY. The excited state is depopulated by both radioactive along non-radioactive repeated mixing. Therefore, the PLQY is alternatively described in the form of the ratio between radioactive repeated mixing speed and whole mixing speed [29]:

$$\text{PLQY} = \frac{\Gamma_{rad}}{\Gamma_{rad} + \Gamma_{non-rad}} \tag{3}$$

where Γ_{rad} and $\Gamma_{non-rad}$, accordingly, stand for radioactive and non-radioactive repeated mixing speed.

The mean amount of time a photon remains within the stimulated status before changing into the ground status is used to calculate the

excited state lifespan. The mean lifespan is determined by a sole exponential fitting, and it would be the opposite in relation to the overall repeated mixing speed. Consequently, the equation below is used to calculate lifespans:

$$\tau_{ave} = \tau = \frac{1}{\Gamma_{rad} + \Gamma_{non-rad}} \quad (4)$$

where τ_{ave} represents the typical lifespan. Consequently, the following formula may be used to determine the radiative and nonradiative recombination rates [30]:

$$\Gamma_{rad} = \frac{\text{PLQY}}{\tau} \quad (5)$$

$$\Gamma_{non-rad} = \frac{1 - \text{PLQY}}{\tau} \quad (6)$$

Within the small-stimulation domain, the luminescent intensity would be typically proportional to $\sigma\Phi N\tau_{\max}/\tau_{rad}$ (i.e., $\sigma\Phi N(PLQY)$) with σ being the stimulation cross section, Φ being the photon flux, and N being the quantity for optically functional centers, in turn. The proportions for functional ions of Mn^{4+} within these specimens is approximated using the formulas given below, assuming that all specimens have the same σ [31]:

$$\frac{N_i}{N_1} = \frac{I_i \times (\text{PLQY})_i}{I_1 \times (\text{PLQY})_1} \quad (7)$$

3.2. WLED's properties with varying SiO_2 amount in K_2SiF_6:Mn^{4+}@SiO_2 compound

Fig. 3 presents the calculated scattering coefficients for SiO_2 particles with the wavelength 400-800 nm. Based on various concentration of the SiO_2 volumes (5% - 10% - 15%), we have the scattering coefficients of 1-4 mm^{-1}, 2-9 mm^{-1}, 4-14 mm^{-1}, respectively. The scattering coefficient would be proportional to the particles' presence, meaning that scattering coefficients surge after raising the SiO_2 volumes.

With the presence of KMnSF@SiO_2 compound, the transmission power of the WLED package collected under 460-nm blue excitation source is presented in Fig. 4. At different dosages of the SiO_2 (5 wt.%, 10 wt.%, and 15 wt.%), visible emission bands with maximum points at about 460 nm and 600 nm are seen with minor changes in position, shape, and intensity. Such an inclusion of blue and orange-red emission peaks in the LED output implies that the scattering of SiO_2 will not hinder the strength of light output while supporting to enhancing the device's color properties, such as color rendering index (CRI), variation of the angular correlated color temperature (CCT), and color quality scale (CQS) [32].

Fig. 5 illustrates the color variations (CCT) depending on the SiO_2 volumes in the phosphor layer KMnSF@SiO_2. The CCT value reaches the peak at nearly 3250 K, reaches the second highest point at over 3150 K when the volumes are 0 and 5 wt.%, respectively. It reaches the smallest points at around 2950 - 3000 K when the particle is 15 wt.%. It may be claimed that with the proper volumes for SiO_2 in the layer of 0 - 5 wt.%, the CCT value will be at its highest.

Subsequently, Fig. 6 shows the color deviation variations (D-CCT) depending on the SiO_2 amounts. The D-CCT values reach the peaks at 180 – 220 K when the particle amounts are up to 5 wt.%. It hits the smallest point at 50 K when the SiO_2 percentage is 10 wt.%. Accordingly, the SiO_2 presence can result in the lowest D-CCT value or the greatest color-dispersion uniformity with the appropriate weight percentage of 10 wt.%.

Fig. 7 reveals the illuminating beam from the LED as a function of SiO_2 weight percentages. When the particle volumes are 0 – 5 wt.%, there are maximum lumen values at nearly 73.5. On the other hand, the lumen value is just around 71 when the content of SiO_2 is 15 wt.%. Thus, the SiO_2 weight percentages of 0 – 5 wt.% will be the most suitable for lumen output.

Figs 8 and 9 show the changes of CRI and CQS values, in turn. Both CRI and CQS values tend to go down when the scattering particle SiO_2 percentages get larger. The CRI value decreases from 56.2 to 55.9 when the particle amount surges (0 - 15 wt.%). Additionally, the growth of SiO_2 percentages induces the decline

in CQS value, from about 42.5 at 0-wt.% SiO_2 to about 34 at 50-wt.% SiO_2.

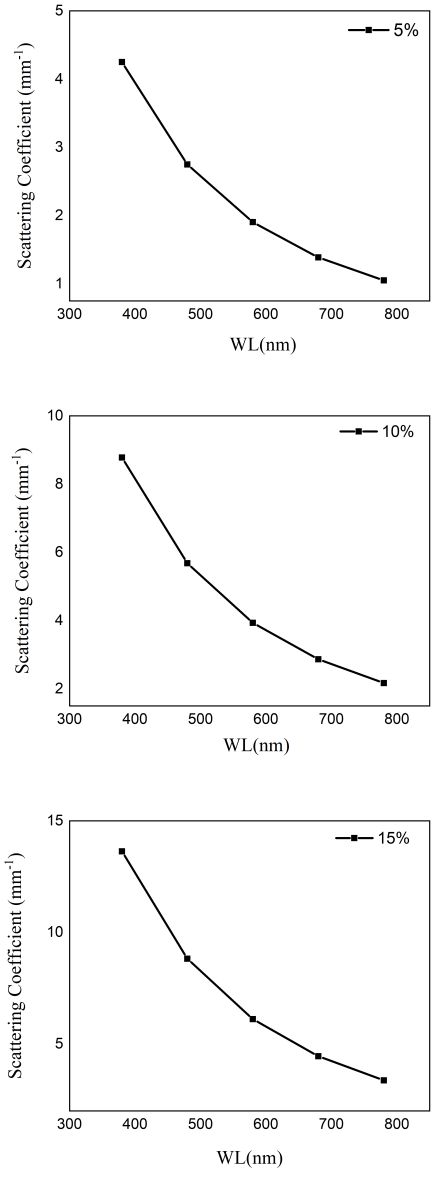

Fig. 3: Scattering coefficients of SiO_2 particles at (a) 5%, (b) 10%, (c) 15%.

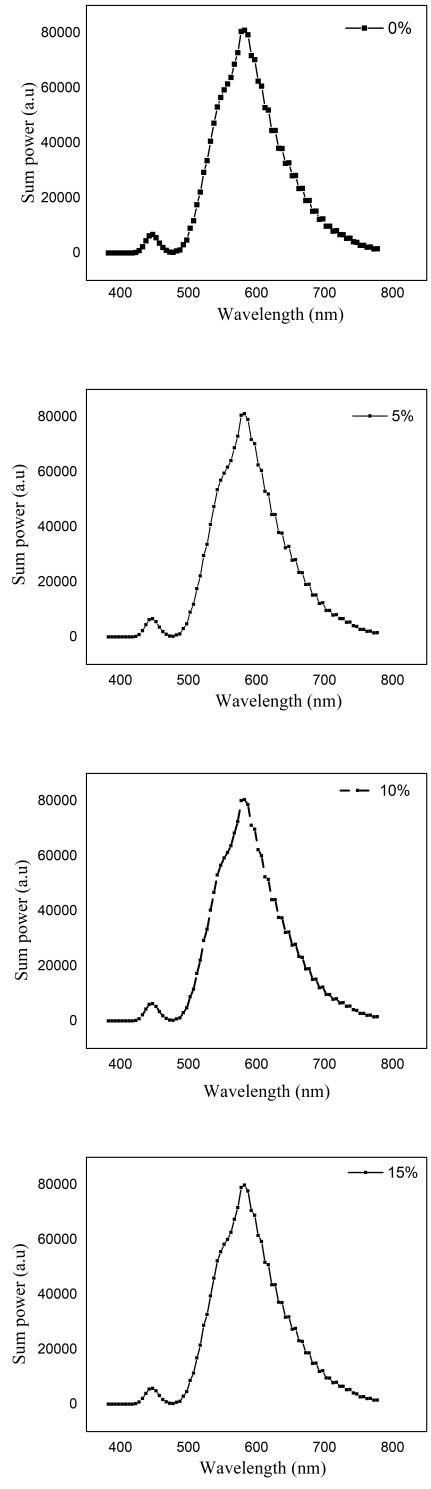

Fig. 4: Spectrum color range with various SiO_2 weight percentages at (a) 0%, (b) 5%, (c) 10%, (d) 15%.

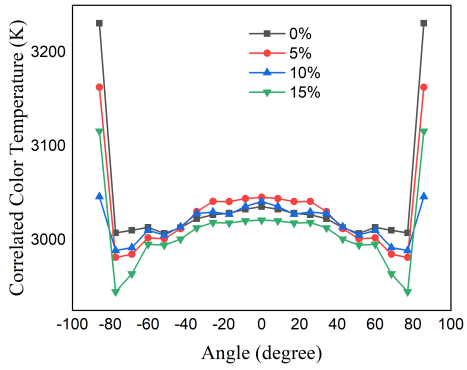

Fig. 5: The CCT variations according to SiO_2 weight percentages.

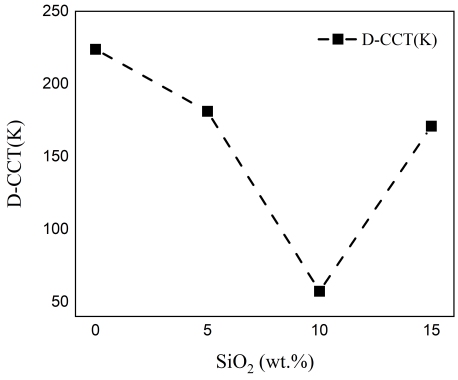

Fig. 6: Investigation of the color deviation changes according to SiO_2 weight percentages.

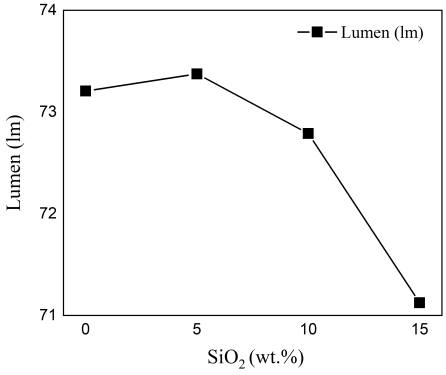

Fig. 7: The luminous flux emitted by the LED according to various weight percentages of SiO_2.

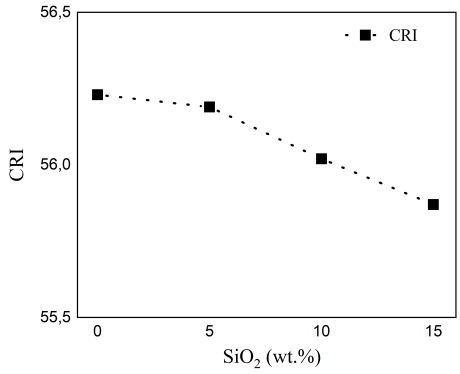

Fig. 8: The CRI variations according to SiO_2 weight percentages.

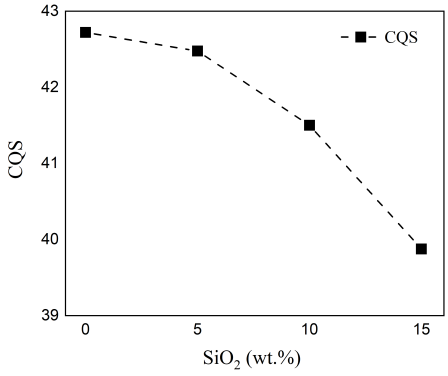

Fig. 9: The CQS variations according to SiO_2 weight percentages.

4. Conclusions

In conclusion, using microfluidic technology, we were able to produce K_2SiF_6:Mn^{4+} phosphors with remarkably consistent particle size and shape. Because the study did not employed the HF compound throughout the test, the danger to the testing procedure was significantly lower. With the duct having 4-mm diameter as well as administration rate under 1000 μL/min, the specimen was the most homogeneous, demonstrating that the right duct diameter along with administration rate may encourage the creation for phosphor granules.

The WLED utilizing K_2SiF_6:Mn^{4+} coupled with YAG:Ce^{3+} and SiO_2 scattering particles exhibits blue and red emission peaks in the visible wavelength. The scattering of light in the phosphor layer increases on the higher SiO_2 weight percentages. Under the same condition, a small CCT at around 3200 K is achieved with low D-CCT value, showing the potential of KMnSF@SiO_2 in fabricating WLED models. The lumen output of the WLED also shows increased values with small-volume SiO_2 in the layer. However, the scattering of SiO_2 does not favor the color rendering factors, showing a decline in both CRI and CQS at higher SiO_2 percentages.

Shortly, the findings demonstrate the significant potential of microfluidic technology for homogenizing elevated-performance K_2SiF_6:Mn^{4+} phosphors. Additionally, it demonstrates the promising prospect of the proposed phosphor compound with SiO_2 scattering particles to improve the luminous flux and angular uniformity of the WLED. The study can also serve as a valuable reference for further investigations on materials and structures for higher-performance WLED devices.

References

[1] Chou, L., Wu, S., Hung, H., Lin, W., Z.P., C., Ivanov, A., & Chia, S. (2022). Compact multicolor two-photon fluorescence microscopy enabled by tailorable continuum generation from self-phase modulation and dispersive wave generation. *Optics Express*, *30*, 40315.

[2] Fjodorow, P., Frolov, M., Korostelin, Y., Kozlovsky, V., Schulz, C., Leonov, S., Skasyrsky, Y., & Yuryshev, N. (2022). Intracavity absorption spectroscopy of HCl isotopes, H_2O, CH_4, C_2H_4, and C_2H_6 in the 3.1–3.4 μm spectral range using a Cr:CdSe laser. *Optics Express*, *30*, 40347.

[3] Lv, C., Li, C., Xiao, K., & Gao, C. (2022). Interim connection space based on colorimetric values for spectral image compression and reproduction. *Optics Express*, *30*, 40144.

[4] Li, Y., Shi, X., Yang, L., Pu, C., Tan, Q., Yang, Z., & Huang, H. (2022). Multilayer collaborative generative adversarial transformer for cholangiocarcinoma classification from hyperspectral pathological images. *Biomedical Optics Express*, *13*, 5794.

[5] Wei, Y., Zhao, M., & Yang, Z. (2022). Silicon metasurface embedded Fabry–Perot cavity enables the high-quality transmission structural color. *Optics Letters*, *47*, 5344.

[6] Lu, Q., Ding, Y., Wang, W., Liu, S., & Xu, M. (2022). VIS-NIR superachromatic triplet design with five-color correction for a broadband interferometer. *Applied Optics*, *61*, 8880.

[7] Bogh, C.L., Muhowski, A.J., Nelson, M.D., Rodgers, V.G.J., & Prineas, J.P. (2022). Measurement of recombination mechanisms in mid-infrared W-superlattices. *Optical Materials Express*, *12*, 4261.

[8] Zhang, Y., Wu, Z., Lin, P., Pan, Y., Wu, Y., Zhang, L., & Huangfu, J. (2022). Hand gestures recognition in videos taken with a lensless camera. *Optics Express*, *30*, 39520.

[9] Xu, H., Hong, F., Liu, G., Dong, X., Yu, W., & Wang, J. (2020). Green route synthesis and optimized luminescence of K_2SiF_6:Mn^{4+} red phosphor for warm WLEDs. *Optical Materials*, *99*, 109500.

[10] Huang, L., Zhu, Y., Zhang, X., Zou, R., Pan, F., Wang, J., & Wu, M. (2016).

HF-Free hydrothermal route for synthesis of highly efficient Narrow-Band red emitting phosphor K_2SI_1–XF_6:XMn^{4+} for warm White Light-Emitting diodes. *Chemistry of Materials*, *28*, 1495—-1502.

[11] Fan, C., Zhao, H., Zhao, Z., Li, J., Du, Y., Yang, X., & Zhang, L. (2022). Single-shot quantitative phase imaging with phase modulation of a liquid crystal spatial light modulator (LC-SLM) under white light illumination. *Optics Letters*, *47*, 5264.

[12] Li, G., Liu, Y., Xu, Q., Liang, H., & Wang, X. (2022). Deep learning enabled inverse design of nanocrystal-based optical diffusers for efficient white LED lighting. *Applied Optics*, *61*, 8783.

[13] Zhu, X., Wang, G., Luo, X., Zhang, J., Liu, J., & Guo, X. (2020). Angular color uniformity enhancement for Color-Mixed LEDs by introducing a diffusing coating layer. *IEEE Photonics Journal*, *12*, 1—12.

[14] Yu, S., Li, Z., Liang, G., Yu, B., & Chen, K. (2016). Angular color uniformity enhancement of white light-emitting diodes by remote micro-patterned phosphor film. *Photonics Research*, *4*, 140–145.

[15] Lee, T.X. & Huang, Y.C. (2018). Simultaneously improve White LED Omni-Directional package efficacy and spatial color uniformity on scattered photon extraction technology. *Crystals*, *9*, 21.

[16] Das, S., Lenka, T.R., Talukdar, F.A., Velpula, R.T., & Nguyen, H.P.T. (2023). Design and Analysis of Novel High-Performance III-Nitride MQW-based Nanowire White-LED using HfO_2/SiO_2 Encapsulation. *Optical and Quantum Electronics*, *55*, 67.

[17] Zhou, S., Liu, M., Xu, H., Liu, Y., Gao, Y., Ding, X., Lan, S., Fan, Y., Gui, C., & Liu, S. (2019). High-efficiency GaN-based LED with patterned SiO_2 current blocking layer deposited on patterned ITO. *Optics & Laser Technology*, *109*, 627–632.

[18] Li, Z., Li, J.X., Li, J., Deng, Z., Deng, Y., & Tang, Y. (2020). Scattering effect on optical performance of Quantum Dot White Light-Emitting diodes incorporating SIO_2 nanoparticles. *IEEE Journal of Quantum Electronics*, *56*, 1—9.

[19] Domański, G., Konarzewski, B., Pawłowski, Z., Zaremba, K., Marzec, J., Trybuła, A., & Kurjata, R. (2007). The use of the Monte Carlo method to determine optical parameters of tissue," Polish Journal of Medical Physics and Engineering. *Polish Journal of Medical Physics and Engineering*, *13*, 23–32.

[20] Metropolis, N. & Ulam, S.M. (1949). The Monte Carlo method. *Journal of the American Statistical Association*, *44*, 335—-341.

[21] Zhu, C. & Liu, Q. (2013). Review of Monte Carlo modeling of light transport in tissues. *Journal of Biomedical Optics*, *18*, 050902.

[22] Moradi, M. & Chen, Y. (2023). Monte Carlo Simulation of diffuse optical spectroscopy for 3D modeling of dental tissues. *Sensors*, *23*, 5118.

[23] Mao, J., Ling, Y., Xue, P., & Su, Y. (2022). Monte Carlo-based full-wavelength simulator of Fourier-domain optical coherence tomography. *Biomedical Optics Express*, *13*, 6317.

[24] Carles, G., Zammit, P., & Harvey, A. (2019). Holistic Monte-Carlo optical modelling of biological imaging. *Scientific Reports*, *9*, 15832.

[25] Nguyen, A.H., Ly, K.L., Li, C.Q., & Wang, Z. (2022). Single-shot 3D shape acquisition using a learning-based structured-light technique. *Applied Optics*, *61*, 8589.

[26] Chen, L., Lee, Z., Lin, G., Wang, Y., Wang, J., & Lai, W. (2022). On the measurement of remote sensing reflectance by a traditional above-water approach in small water bodies. *Applied Optics*, *61*, 8664.

[27] Chen, J., Wang, A., Pan, A., Zheng, G., Ma, C., & Yao, B. (2022). Rapid full-color

Fourier ptychographic microscopy via spatially filtered color transfer. *Photonics Research*, *10*, 2410.

[28] Liu, C., Zou, Z., Miao, Y., & Qiu, J. (2022). Light field quality assessment based on aggregation learning of multiple visual features. *Optics Express*, *38298*, 30.

[29] Kumari, A., Nayak, P., Patra, B., Venkatasubbaiah, K., & Das, R. (2022). Third-order nonlinear optical manifestations in an intramolecular proton transfer fluorophore due to Tamm-plasmon based broadband optical absorbers. *Journal of the Optical Society of America B*, *39*, 2857.

[30] Lin, S., Sun, P., Gao, H., & Ju, Z. (2022). Haze optical-model-based nighttime image dehazing by modifying attenuation and atmospheric light. *Journal of the Optical Society of America A*, *39*, 1893.

[31] Liang, H., Yang, G., Bai, S., Li, C., Li, X., Wang, Y., Huang, J., Ji, J., & Zhu, Y. (2022). Efficient and tunable photoluminescence for terbium-doped rare-earth-based Cs_2NaYCl_6 double perovskite. *Optics Letters*, *47*, 5176–5179.

[32] Cao, X., Lian, Y., Liu, Z., Zhou, H., Wang, B., Zhang, W., & Huang, B. (2022). Hyperspectral image super-resolution via a multi-stage scheme without employing spatial degradation. *Optics Letters*, *47*, 5184–5187.

About Authors

Sang Dang HO was born in Ho Chi Minh City, Vietnam in 1973. He received the M.Ss. degree in Electrical Engineering from Ho Chi Minh University of Technology, Ho Chi Minh City, Vietnam in 2008, and received the Ph.D. degree in Electrical Engineering from VSB-Technical University of Ostrava, Czech Republic, in 2020. Presently, he is working as a lecturer at the Faculty of Electrical and Electronics Engineering, Ton Duc Thang University, Ho Chi Minh City, Vietnam. He is currently pursuing the Ph.D. degree in electrical engineering at VSB-Technical University of Ostrava, Czech Republic. His research interests involve the optimization of the power system and applications of soft computing in control of electric machine drives and optics science. He can be contacted at email: hodangsang@tdtu.edu.vn.

Nguyen Thi Phuong LOAN was born in Da Nang province. In 2006, She received her master degree from University of Natural Sciences. Her research interest is optoelectronics. She has worked at the Faculty of Fundamental 2, Posts and Telecommunications Institute of Technology, Ho Chi Minh City, Vietnam. She can be contacted at email: ntploan@ptithcm.edu.vn.

Hsiao-Yi LEE was born in Hsinchu city, Taiwan. He has been working at the Department of Electrical Engineering, National Kaohsiung University of Science and Technology, Kaohsiung, Taiwan. His research interest is optics science. He can be contacted at email: leehy@nkust.edu.tw.

Nguyen Doan Quoc ANH was born in Khanh Hoa province, Vietnam. He has been working at the Faculty of Electrical and Electronics Engineering, Ton Duc Thang University. Quoc Anh received his PhD degree from National Kaohsiung University of Science and Technology, Taiwan in 2014. His research interest is optoelectronics. He can be contacted at email: nguyendoanquocanh@tdtu.edu.vn.